Optics & Laser Technology 164 (2023) 109540

Contents lists available at ScienceDirect

Optics and Laser Technology

journal homepage: www.elsevier.com/locate/optlastec

Full length article

Enhancing resolution of terahertz imaging systems below the diffraction limit

Jaime Calvo-Gallego [a,*], Juan A. Delgado-Notario [a], Oleg V. Minin [b], El Hadj Abidi [a], Miguel Ferrando-Bataller [c], Kristel Fobelets [d], Jesús E. Velázquez-Pérez [a], Igor V. Minin [b], Yahya M. Meziani [a]

[a] Nanotechnology Group, USAL-Nanolab, Universidad de Salamanca, Plaza de la Merced, Edificio Trilingüe, 37008 Salamanca, Spain
[b] Tomsk Polytechnical University, 30 Lenin Avenue, Tomsk 634050, Russia
[c] Department of Communications, Telecommunication Engineering School, Universitat Politècnica de València, 46022 Valencia, Spain
[d] Department of Electrical and Electronic Engineering, Imperial College, South Kensington Campus, London SW7 2AZ, United Kingdom

ARTICLE INFO

Keywords:
Diffraction limit
Image contrast
Terahertz detectors
Terajet effect
Terahertz imaging systems

ABSTRACT

We report on resolution enhancement of sub-terahertz (THz) images by using the terajet effect. A mesoscale cuboid dielectric particle, used to establish the terajet, was placed in front of an object located at the focus of the THz beam. The object under study was based on a printed circuit board (PCB) perforated with different holes with diameters ranging from 1.8 to 3.0 mm and separated from each other by a distance that varies from 0.25 to 4 mm. The sample was illuminated by a continuous wave source at a frequency of 0.3 THz and the image was obtained using a sensor based on a strained-Si Field-Effect Transistor. The image was formed pixel-by-pixel in a transmission mode configuration. A clearer image with enhanced resolution was obtained when the mesoscale cube was introduced in the optical path. The terajet effect made possible to resolve a separation between holes of around 0.5 mm (lower than the wavelength, 1 mm), that is, below the diffraction limit. The method described is easy to implement, cost effective and could be used to improve the resolution of any real imaging system.

1. Introduction

Terahertz (THz) technology has gained increasing interest in the last decades due to its potential applications [1,2] like: inspection and security (most of materials are transparent to this radiation), communications (possibility of very high data rate transmission), spectroscopy (many chemical species have spectral fingerprints in the THz region), etc. The THz region of the electromagnetic spectrum is located between the infrared and the RF/microwaves ones and, accordingly, the THz region bridges Electronics (limited by the cut-off frequency of transistors) and Photonics (limited by the low energy of photons). Imaging is among the most sought applications that THz technology [3] and refs therein] can enable in medicine, biophotonics, inspection and security [4–7]. Nevertheless, THz imaging suffers from low spatial resolution as compared to imaging in the UV and visible spectral ranges due to its comparatively large wavelength (0.3–3 mm (0.1 −10THz)) and the fundamental diffraction limit. Different techniques were proposed to improve the resolution like near-field scanning [8], aspherical lenses [9], solid immersion [3,10], THz microjets with dielectric spherical particles [11], neural networks [12], structured illumination [13] and, also, the use of different methods of numerical analysis [14–17]. Very recently, a wide field of view aspheric lens with a diameter of 264 mm has been used in a THz imaging system at 0.1 THz allowing rapid imaging with extended depth-of-field (DOF) to 85 mm [18]. Also, recently the terajet effect was proposed and demonstrated to improve the efficiency of the coupling of the electromagnetic radiation and, hence, to increase both the sensitivity of terahertz detectors [19–20] and the spatial resolution of the THz imaging systems [21–22]. The physics of the formation of a sub-diffraction spot of a mesoscale particle (dimensions about 1 to 5 times the size of the wavelength) of an arbitrary three-dimensional shape is based on the well-known effect of a photonic jet (in this paper a photonic jet in the THz range), a specific type of

* Corresponding author.
E-mail addresses: jaime.calvo@usal.es (J. Calvo-Gallego), juanandn@usal.es (J.A. Delgado-Notario), ovminin@tpu.ru (O.V. Minin), elhadjabidi@usal.es (E. Hadj Abidi), mferrand@dcom.upv.es (M. Ferrando-Bataller), k.fobelets@imperial.ac.uk (K. Fobelets), js@usal.es (J.E. Velázquez-Pérez), ivminin@tpu.ru (I.V. Minin), meziani@usal.es (Y.M. Meziani).

https://doi.org/10.1016/j.optlastec.2023.109540
Received 22 November 2022; Received in revised form 20 January 2023; Accepted 26 April 2023
Available online 6 May 2023

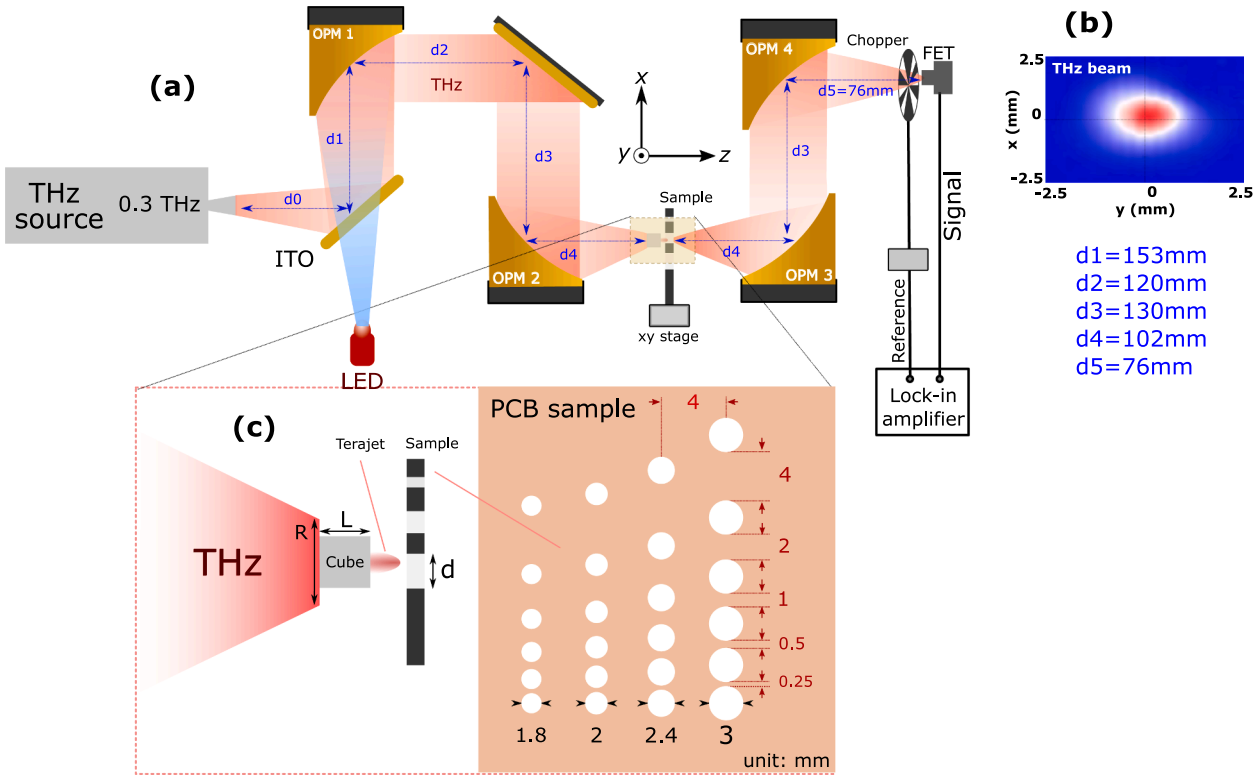

Fig. 1. (a) Schematic description of the imaging setup with the separation distances between the different components. The distances d1, d5 and d5 are the focal points of the OPM1, OPM2&3 and the OPM4, respectively. The THz image was pixel-by-pixel generated in a transmission configuration. (b) The measured spatial beam profile of the THz spot without the use of the cuboid and (c) the illustration of the terajet effect and the manufactured PCB with hole diameters and their separation. The following abbreviations were used, OPM: Off-axis Parabolic Mirror, ITO: Indium Tin Oxide, FET: Field Effect Transistor, LED: Light Emitting Diode. (single column fitting image) (colour should be used for this figure in print).

electromagnetic beam focused in the near-field area of the particle [23]. It's formed upon the incidence of a plane wave on the arbitrary particle (a cuboid-shaped mesoscale particle in this work). The radiation propagates through the particle and near its edge with a phase velocity higher at the edge than in the centre. The focused beam has the advantage of being smaller in size (could be smaller than the diffraction limit) and with higher intensity than the original one. In general, this effect provides a simple method to improve the focusing of the THz beam by simply placing a low-loss dielectric particle with wavelength-scaled dimensions in front of the detector. This makes possible to localize the radiation incident on the detector to sub-wavelength volumes and, thus, overcoming the diffraction limits, matching the size of the field localization region and the size of the sensitive part of field-effect transistors (FETs) or point-contact detectors. It was demonstrated the terahertz scanning microscopy feature at 0.3 THz using a dielectric cuboid probe [24].

In the present work, we report on an experimental demonstration of the resolution enhancement of THz imaging systems using the terajet effect at 0.3THz ($\lambda = 1$ mm). A three-wavelength length particle (in the present case, a Teflon cube) was used to localize the incident radiation to a subwavelength volume and focus the beam directly onto the object. A strained-silicon modulation FET was used as a direct detector of the incident beam. A clear improvement of the resolution of the terahertz image was obtained when the cube was placed in the focal point of the THz beam in front of the object. The terajet effect made possible to distinguish two holes separated by 0.25 to 0.5 mm ($0.2{\cdot}\lambda - 0.4{\cdot}\lambda$) in air, which is beyond the Rayleigh's criterion, with an enhancement contrast up to 14. This demonstrates the ability of the method to simultaneously overcoming the diffraction limit and enhancing the spatial resolution of terahertz imaging systems.

2. Methods

The schematic description of the imaging setup is shown in Fig. 1-(a). The continuous wave terahertz source is based on a solid-state harmonic generator with an output power of 6 mW at 0.3 THz. The emitted power was measured close to the output of the source using a highly calibrated pyroelectric detector (it's a THz-20 from SLT Sensor with an aperture of 20 mm and responsivity of 140 V/W at a frequency of 1.4THz. The detector was calibrated at the National Metrology Institute of Germany[1]). A visible Light Emitting Diode (LED) in combination with an indium tin oxide (ITO) mirror was used for the alignment of the THz beam. This latter was optically modulated by a chopper at a rate of 298 Hz and used as the reference for a lock-in amplifier (a Stanford Research SR830 lock-in amplifier with a 10 MΩ input impedance and sensitivity of 2 nV). The THz output beam was firstly collimated and focused into the sample by a planar mirror followed by two gold-coated off-axis parabolic mirrors (OPM1 & 2). Fig. 1-(b) shows the beam spot where no cube was introduced in the optical path. Here, to improve the imaging resolution, a Teflon mesoscale particle (the material was manufactured by Broncesval[2]) shaped as a cube with 3 mm edge length was placed in the first focal point of the beam, after the OPM2, and in front of the sample under imaging. The cube was fabricated using a computer numerical control (CNC) machine on a Teflon base with a thickness of 1 mm. Teflon is a common material widely used in the terahertz range because of its low absorption loss in this range. It's also possible to use other type of

[1] More info in https://www.pyrosensor.de/Standard-924644.html.

[2] https://www.broncesval.com/en/plastics-technicians/ptfe-teflon-polytetrafluoroethylene/ The properties of the Teflon subsequently used in simulations were: refractive index n= 1.41 [25], permittivity, ε_r, of 2.05±0.01 and a low loss tangent of $(2.7\pm0.2)\times10^{-4}$ measured at 84GHz [26].

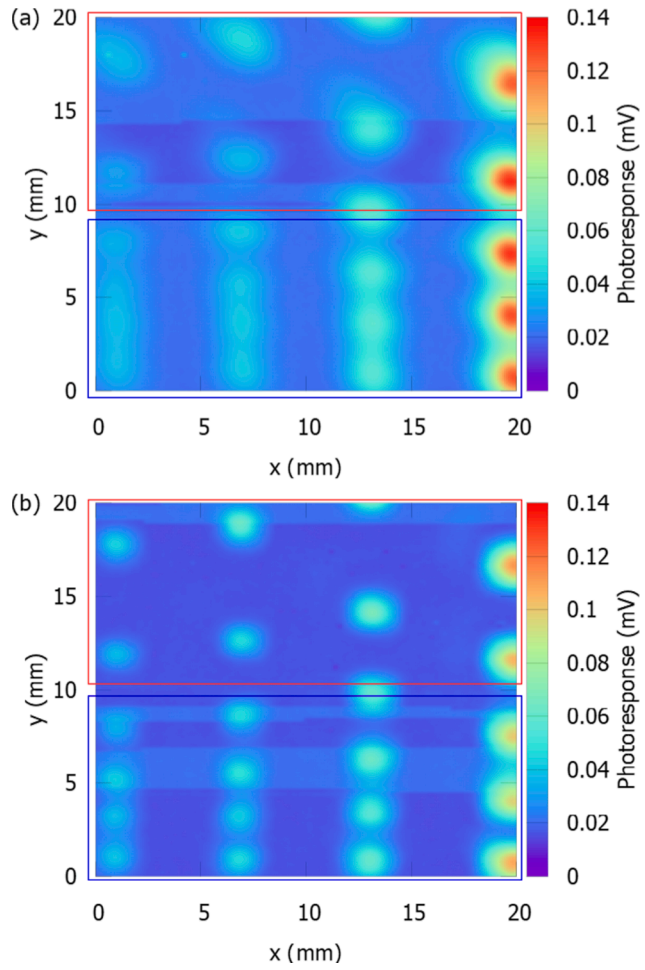

Fig. 2. Image obtained under excitation of 0.3 THz (a) without the cube and (b) with the cube. XY plane refers to PCB on Fig. 1. (single column fitting image) (colour should be used for this figure in print).

materials like Polystyrene [27] and paraffin, among others. The study of the photonic jet (so-called terajet in the THz range) has been performed in the optical range of the electromagnetic spectrum using different structures: micro two dimensional scaled cylindrical [28] and three dimensional spherical [29] dielectrics. It was demonstrated in [30] that the beam spot localization depends upon the refractive index of the material. By increasing the refractive index (*n*), the terajet beam moves inside the particle while for smaller *n*, the beam is driven off the particle and exhibits a reduced power density. A cuboid made of Teflon (n = 1.4) [30] allows to achieve high intensity maximum of the terajet beam power that is located at the shadow of the particle.

The THz beam was again collimated and focused a second time into the detector by using OPM3 & 4. A strained Si/SiGe modulation FET (MODFET) [31–32] was used to detect the 0.3 THz radiation. This device has been actively investigated and validated as an efficient room temperature detector. It shows competitive responsivity (~5V/W), low noise equivalent power (NEP) (~100 pW/Hz$^{1/2}$) and fast time response [33]. The photoresponse signal generated by the incoming THz radiation was collected on the drain contact and measured by the lock-in amplifier. An average of 20 measurements was taken for each position to reduce measurements fluctuation. The 0.3 THz image was generated in a transmission mode configuration and the object was moved in the x-y plane by an automated linear stage motor to generate a pixel-by-pixel image. A Thorlabs LTS300 x-y stage was used to move the sample in the x-y plane (the stage has a bidirectional repeatability and a backlash of around 2 μm).

A standard printed circuit board (PCB) with a thickness of 1.5 mm including the copper layer (Fig. 1-(c)) was chosen as subject for the imaging system. The thickness of the copper layer, 35 μm, is much larger than the skin depth of copper (~0.2 μm) at 0.3 THz what guarantees that the THz radiation is completely blocked by the copper layer and no interferences were expected. The sample was perforated in a set of four columns of holes with diameters ranging from 1.8 mm to 3 mm. Hole columns were equally separated by a 4 mm in the horizontal direction (Fig. 1). Within each column, the vertical spacing between holes of the same diameter was progressively reduced from 4 mm down to 0.25 mm. The PCB board was fabricated by a CNC machine with a precision of 25 μm. This design gives a simple method to investigate the resolution of the imaging system.

3. Results and discussions

Fig. 2(a) shows the THz image obtained when no cube was placed in the optical path of the imaging setup i.e., it corresponds to a conventional image obtained in a standard THz imaging system. The separation between holes of 3 mm in diameter - especially the ones separated at 4 and 2 mm - can be clearly appreciated in the THz image (red rectangle in Fig. 2(a)). However, when the diameter of the holes is reduced from 3 mm down to 1.8 mm, neither the holes nor their spacing are properly resolved and, accordingly, it is almost impossible to distinguish the circular shape and the existence of a spacing between adjacent holes as the separation is below the wavelength (blue rectangle in Fig. 2(a)). Subsequently, the Teflon cube was placed at the first focus and in front of the PCB (the distance to the cube to the PCB was less than 1 mm) and a THz image, Fig. 2(b), was generated following the same procedure described previously. In comparison with the first THz image, where no cube was used, Fig. 2(b) shows a clear enhancement of the image resolution. The holes with diameters of 1.8 mm are now well resolved (blue rectangle in Fig. 2(b)). In the THz image it is easy to identify the smaller holes (d = 1.8 mm) and the 0.25 mm spacing that is below the radiation wavelength. The spatial resolution of an optical system is usually limited by the diffraction of the THz beam on its optical elements. The spatial resolution is generally defined by the Rayleigh criterion, [34], (which states that if there is a gap of 20 % in the intensity distribution in the image of two close points, the points will be perceived as separate). Accordingly, the smallest object that a lens can resolve and the smallest diffraction limited spot that the collimated beam can focus the light on is given by $\delta = 1.22 \bullet \lambda \bullet F/D$, where F and D are the focal length and diameter of the lens, respectively. Therefore, the smallest resolvable spot is comparable to or larger than the wavelength of the THz beam.

The introduction of the cube leads to the formation of the terajet beam in the shadow surface of the mesoscale particle [30]. The terajet effect localize the beam in a small volume (of a size comparable or lower than the one determined by the wavelength) and with higher intensity than the incident THz wave. It has already been demonstrated [20,35–36] that the terajet effect can considerably enhance the resolution of imaging systems and, specially, those operating in the terahertz range in which the spatial resolution is limited by the relatively high value of the wavelength.

Full-wave electromagnetic simulations were performed using the finite integral technique in the commercial software CST[3]. These simulations allow to electromagnetically analyse large structures when the physical size is much larger than the incident wavelength. The size of the entire structure to be simulated causes CST software to automatically determine the size of the mesh, which has heterogeneous sizes, adapting its dimensions to small and large volumes. In this way, for the simulated structures, the minimum size of the mesh cells was 0.0175 mm and the

[3] CST Studio Suite: https://www.3ds.com/products-services/simulia/products/cst-studio-suite/.

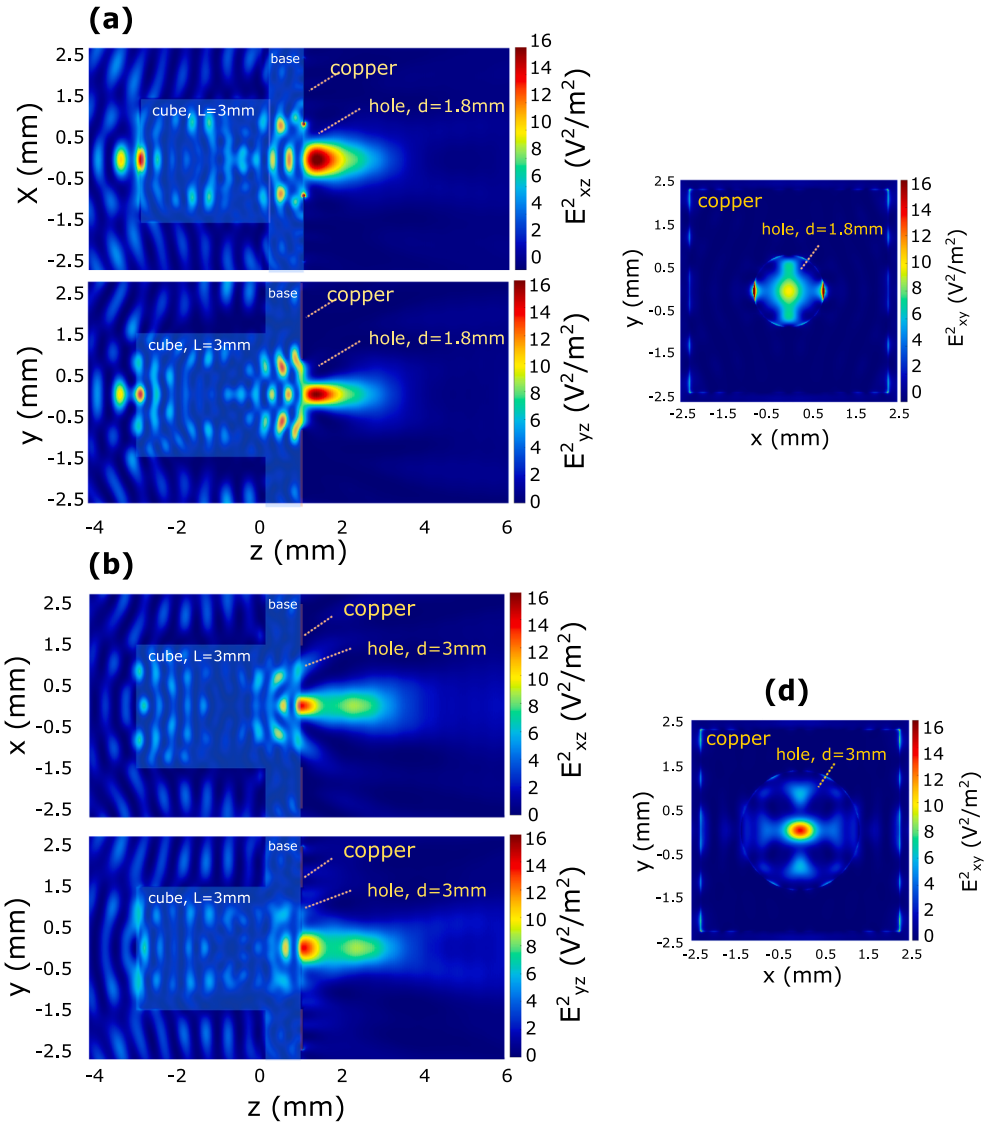

Fig. 3. Normalized electric field strength, obtained by CST simulation, in the xz, yz, and yx planes for two different holes (a) 1.8 mm and (b) 3 mm. For the yx plane, z was fixed at 1.035 mm. (2-column fitting image) (colour should be used for this figure in print).

maximum 0.569758 mm. The impinging 0.3 THz beam was modelled as a plane wave propagating in the *z* direction, perpendicular to both the surfaces of the PCB and the detector, with a linear polarization along the *x* direction. The magnitude of the incident electric field was fixed at E_x = 1 V/m. The cube stretches from *z* = -3 to 0 mm, the base of the cube between *z* = 0 to 1 mm and the PCB (two cases of hole diameter, d = 1.8 or 3 mm, were considered) from *z* = 1 to 1.035 mm (only the copper layer of PCB was considered in simulations). Fig. 3 shows the simulation results of the electric field strength in the *yz* plane normalized to the incident wave at *x* = 0 (Fig. 3(a) and Fig. 3(c)) and at *z* = 1.035 mm (Fig. 3(b) and Fig. 3(d)). The obtained values of the FWHM (Full Width at Half Maximum) along the *x* and *y* directions were 0.8 and 0.5 mm for 3 mm and 1.8 mm hole diameters, respectively. In both cases, it was observed that the THz beam was focused in a smaller area than the incoming one. It had a higher strength, and it was formed at the shadow surface of the cube (as predicted in [30]) and not inside the cube. Simulation results confirm and explain the image resolution enhancement experimentally obtained (Fig. 2). The cross-section of the beam in the *x*-*y* plane perpendicular to the propagation at *z* = 1.035 mm is given in Fig. 3(b) and Fig. 3(d). The cross section of the beam at the rear plane of the object is given in Fig. 3(b) and 3(d) for diameters of 1.8 and 3.0 mm, respectively. The cross-section in Fig. 3(b) exhibits differences in shape and magnitude in comparison with the one given in Fig. 3(d); this is related to the fact that the maximum field strength for the hole with d = 3 mm is not reached at z = 1.392 mm (as for d = 1.8 mm) but at z = 1.035 mm.

Fig. 4 shows vertical cuts along the y direction of the photoresponse signal obtained in the experiments (Fig. 2). The cuts were performed at four × positions (x = 1 mm, 6.8 mm, 13.2 mm, and 19.8 mm) that correspond to the centre of each set of holes. The plots with blue-circle symbols (red/square symbols) show the signal without (with) the cube placed at the first focus. In general, when the cube is inserted in the optical path the photoresponse signal increases and the image resolution is considerably improved producing sharp images of both the holes and the spacing between them. When no cube is used, it's difficult to distinguish and/or separate the closer holes when their diameter and separation are smaller than 2 mm (Fig. 4(a) and Fig. 4(b)). The separation Δx between the edges of the holes was extracted from the maximum values of the photoresponse signal obtained when the cube is present (Fig. 4) using the expression

$$\Delta x = X_{max2} - X_{max1} - d \quad (1)$$

where X_{max2} and X_{max1} are the spatial positions at which the photoresponse exhibits successive adjacent maxima and *d* is the diameter of

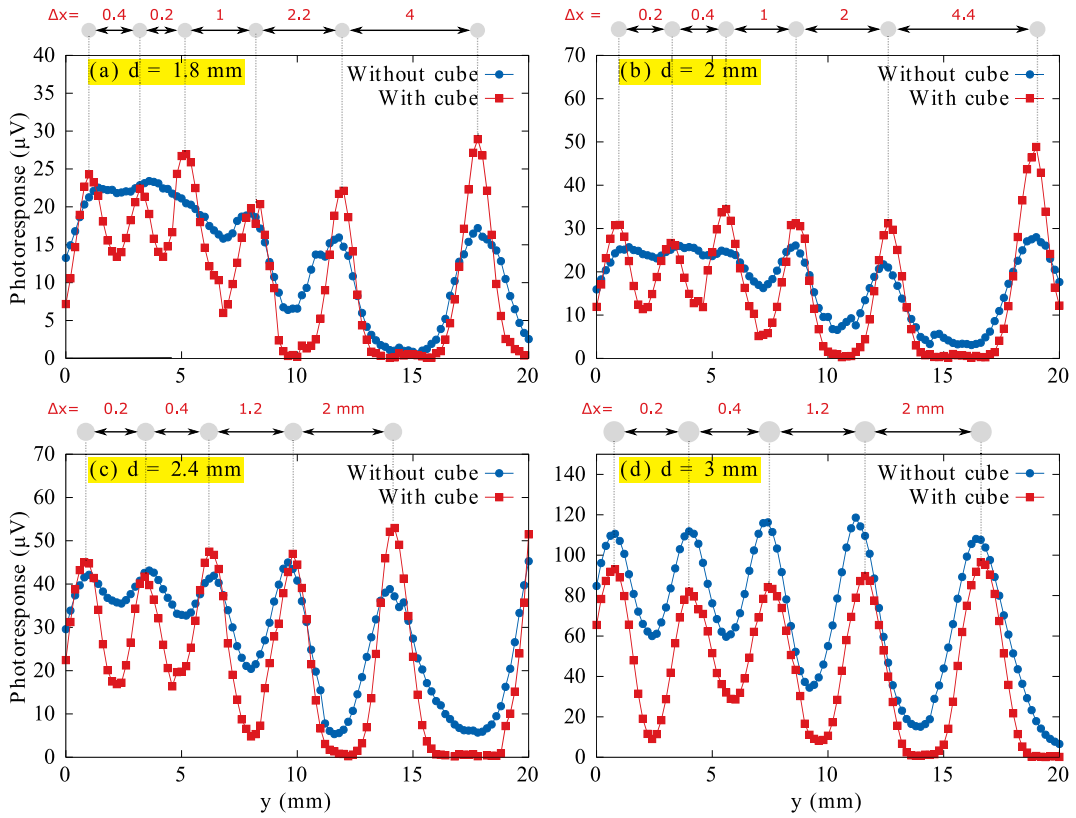

Fig. 4. Photoresponse signal along the y direction at four values of × and four hole diameters: (a) × = 1 mm, d = 1.8 mm (b) × = 6.8 mm, d = 2 mm (c) × = 13.2 mm, d = 2.4 mm and (d) × = 19.8 mm, hole diameter = 3 mm. (2-column fitting image) (colour should be used for this figure in print).

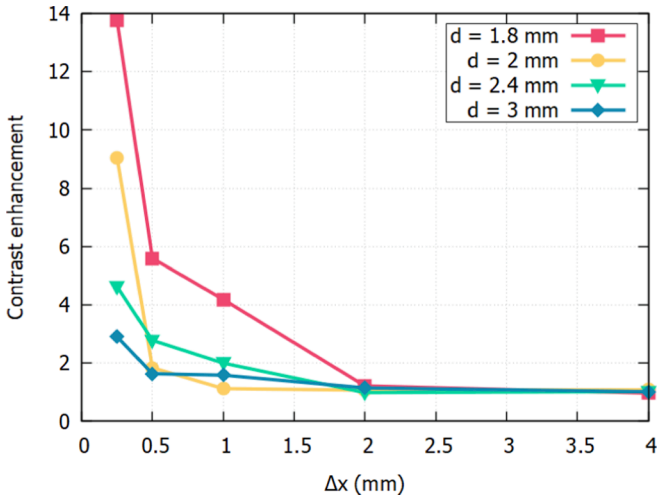

Fig. 5. Contrast enhancement in contrast versus hole separation (Δx) for the four values of hole diameters analysed. (single column fitting image) (colour should be used for this figure in print).

the hole. The obtained values are presented for the four cases in the top of each plot of Fig. 4 and they were comparable to the real ones (shown in Fig. 1) with an estimated error of ± 0.2 mm. These results demonstrate that the terajet effect improves considerably the spatial resolution to a size comparable or lower to the wavelength.

Image contrast allows to quantify the enhancement of the image resolution when the mesoscale cube is used. The contrast was calculated for each hole using the following expression [21]

$$(A_{max} - A_{min})/(A_{max} + A_{min}) \quad (2)$$

where A_{max} and A_{min} are, respectively, the maximum (obtained at the centre of the hole) and the minimum of the photoresponse (obtained in the spacing zone between holes). The contrast enhancement was defined as the ratio between the obtained signal with and without the cube (contrast enhancement = contrast with cube/contrast without the cube)). An enhancement of around 14 was obtained for the smallest hole with d = 1.8 mm) and for separations Δx = 0.25 to 1 mm (Fig. 5). However, for Δx = 2 and 4 mm, the obtained contrast enhancement was close to the unity. Hence, the contrast obtained using the cube is comparable to the one without the cube. This shows that the cube induces an enhancement of resolution for the lower values of the separation and for small holes. However, for the bigger ones, no enhancement of the resolution was observed, and, accordingly, it must be concluded that the use of the cube does not improve the resolution of the imaging system. The fact that the use of the cube only increases the spatial resolution up to a given diameter of the hole is in good agreement with simulations that show that the terajet effect is not significant for large values of the hole diameter. This could be related to some interference between the THz and the terajet beams for holes with diameters higher than 2 mm.

4. Conclusion

An experimental study on the enhancement of the resolution in subterahertz (THz) imaging by using the terajet effect under continuous wave (CW) illumination was presented. To generate the terajet effect a mesoscale Teflon cube was placed in the optical path in front of the object. The dielectric cube allowed to focus the THz beam. The object was a perforated printed circuit board (PCB). The holes had diameters ranging from 1.8 to 3 mm and separated from each other by a distance

that varies from 0.25 to 4 mm. The sample was illuminated by a CW source at a frequency of 0.3 THz and the image was obtained using a strained-Si Field-Effect Transistor as sensor. The image was formed pixel-by-pixel in a transmission mode configuration. Clearer images with enhanced resolution were obtained when a mesoscopic cube was placed in the first focal point to generate the terajet effect compared to the ones obtained using the standard setup in which the dielectric cube was not present. A main result of the work is that the terajet effect made possible to resolve separations between adjacent holes of approximately 0.5 mm (0.5λ), i.e. below the THz light wavelength. 3D full-wave electromagnetic simulations were performed using the finite integral technique to explain experimental results. Simulation results were in good agreement confirming that the contrast enhancement in spatial resolution was associated with the onset on the terajet. Both experimental and theoretical results showed that a contrast enhancement of 14 can be achieved for the smallest value of hole's diameter (1.8 mm) and separation (0.25 mm or 0.25λ) studied. For separations equal or higher than 2 mm (2λ) no contrast enhancement was achieved what is in agreement with simulations that show that the terajet effect is not significant for largest values of the hole's diameter.

Data availability

The data that support the findings of this study are available from the corresponding author upon reasonable request.

CRediT authorship contribution statement

Jaime Calvo-Gallego: Methodology, Software, Validation, Formal analysis, Writing – original draft, Writing – review & editing, Visualization, Supervision. **Juan A. Delgado-Notario:** Methodology, Software, Validation, Formal analysis, Writing – original draft, Writing – review & editing, Visualization, Supervision. **Oleg V. Minin:** Conceptualization, Validation. **El Hadj Abidi:** Methodology, Validation. **Miguel Ferrando-Bataller:** Conceptualization, Methodology, Software, Validation, Formal analysis. **Kristel Fobelets:** Formal analysis, Validation. **Jesús E. Velázquez-Pérez:** Validation, Formal analysis, Writing – original draft, Writing – review & editing, Visualization, Supervision. **Igor V. Minin:** Conceptualization, Validation. **Yahya M. Meziani:** Conceptualization, Methodology, Validation, Formal analysis, Investigation, Writing – original draft, Writing – review & editing, Visualization, Supervision. Jaime Calvo-Gallego and Juan A. Delgado-Notario contributed equally to this work.

Declaration of Competing Interest

The authors declare that they have no known competing financial interests or personal relationships that could have appeared to influence the work reported in this paper.

Data availability

The data that support the findings of this study are available upon reasonable request.

Acknowledgments

This work was partially conducted within the framework of the Tomsk Polytechnic University Development Program. This research was supported by the Spanish Agencia Estatal de Investigación under Grants Numbers PID2019-107885GB-C32, RTI2018-097180-B-100, and PID2021-126483OB-I00, the Consejería de Educación, Junta de Castilla y León under Grant Numbers SA121P20 and SA256P18 and the Universidad de Salamanca Research Program under Grant Number PIC2-2021-02 and the Conselleria de Innovación, Universidades, Ciencia y Sociedad Digital of the Generalitat Valenciana under the Grant Number MFA/2022/056. This work was also supported by Center for Terahertz Research and Applications (CENTERA) project carried out within the International Research Agendas Program for of Foundation for Polish Sciences co-financed by the European Union under the European Regional Development Fund (grant no. MAB/2018/9). IM, OM initiated this work.

References

[1] M. Tonouchi, Cutting-edge terahertz technology, Nature Photon 1 (2) (2007) 97–105.
[2] C. Sirtori, Bridge for the terahertz gap, Nature 417 (6885) (2002) 132–133.
[3] E. Castro-Camus, M. Koch, D.M. Mittleman, Recent advances in terahertz imaging: 1999 to 2021, Appl. Phys. B 128 (2022) 12, https://doi.org/10.1007/s00340-021-07732-4.
[4] C.S. Joseph, A.N. Yaroslavsky, V.A. Neel, T.M. Goyette, R.H. Giles, Continuous wave terahertz transmission imaging of nonmelanoma skin cancers, Lasers Surg. Med. 43 (6) (Aug. 2011) 457–462, https://doi.org/10.1002/LSM.21078.
[5] S. Fan, B.S.Y. Ung, E.P.J. Parrott, V.P. Wallace, E. Pickwell-MacPherson, In vivo terahertz reflection imaging of human scars during and after the healing process, J. Biophotonics 10 (9) (Sep. 2017) 1143–1151, https://doi.org/10.1002/JBIO.201600171.
[6] D.M. Mittleman, Twenty years of terahertz imaging [Invited], Opt. Express 26 (8) (2018) 9417.
[7] H. Guerboukha, K. Nallappan, M. Skorobogatiy, Toward real-time terahertz imaging, Adv. Opt. Photon. 10 (4) (2018) 843.
[8] H.T. Chen, R. Kersting, G.C. Cho, Terahertz imaging with nanometer resolution, Appl. Phys. Lett. 83 (15) (Oct. 2003) 3009, https://doi.org/10.1063/1.1616668.
[9] Y.H. Lo, R. Leonhardt, Aspheric lenses for terahertz imaging, Opt. Express 16 (20) (2008) 15991.
[10] N. V. Chernomyrdin *et al.*, "A potential of terahertz solid immersion microscopy for visualizing sub-wavelength-scale tissue spheroids," in: Unconventional Optical Imaging, May 2018, vol. 10677, p. 70. doi: 10.1117/12.2306132.
[11] M.E. Mitchell, M.H. Bergen, J. Reich, J.F. Holzman, Terahertz Microjets as Realizations of Subwavelength Focusing in the Terahertz Spectrum, IEEE Trans. THz Sci. Technol. 13 (1) (2023) 50–57.
[12] H. Ruan, Z. Tan, Liangtao Chen, Wenjain Wan, Juncheng Cao, "Efficient sub-pixel convolutional neural network for terahertz image super-resolution", Opt. Lett. 47 (2022) 3115–3118.
[13] A. Shayei, Z. Kavehvash, M. Shabany, Improved-resolution millimeter-wave imaging through structured illumination, Appl. Opt. 56 (15) (2017) 4454.
[14] K. Ahi, A method and system for enhancing the resolution of terahertz imaging, Measurement 138 (May 2019) 614–619, https://doi.org/10.1016/J.MEASUREMENT.2018.06.044.
[15] L.-M. Xu, W.-H. Fan, J. Liu, High-resolution reconstruction for terahertz imaging, Appl. Opt. 53 (33) (2014) 7891.
[16] G.C. Walker, J.W. Bowen, J. Labaune, J.-B. Jackson, S. Hadjiloucas, J. Roberts, G. Mourou, M. Menu, Terahertz deconvolution, Opt. Express 20 (25) (2012) 27230.
[17] Y. Liang, W. Fan, and B. Xue, "Image enhancement techniques used for THz imaging," in: International Symposium on Photoelectronic Detection and Imaging 2011: Terahertz Wave Technologies and Applications, Jun. 2011, vol. 8195, p. 819515. doi: 10.1117/12.900775.
[18] X. Hu, X. Wang, S. Liu, W. Lin, Y. Geng, X. Chai, B. Gu, Research on long-distance, wide field-of-view and large depth-of-field terahertz imaging based on aspheric lens, Optics and Lasers in Engineering 161 (2023), 107381, https://doi.org/10.1016/j.optlaseng.2022.107381.
[19] I. V. Minin, et al., "Responsivity enhancement of a strained silicon field-effect transistor detector at 03 THz using the terajet effect," Opt. Lett., vol. 46, no. 13, p. 3061, Jul. 2021, doi: 10.1364/OL.431175.
[20] O.V. Minin, I.V. Minin, Y.M. Meziani, S. Hisatake, Improvement of a point-contact detector performance using the terajet effect initiated by photonics, Opt. Eng. 60 (08) (Oct. 2020), 082005, https://doi.org/10.1117/1.OE.60.8.082005.
[21] H.H. Nguyen Pham, S. Hisatake, O.V. Minin, T. Nagatsuma, I.V. Minin, Enhancement of spatial resolution of terahertz imaging systems based on terajet generation by dielectric cube, APL Photonics 2 (5) (2017) 056106.
[22] V. Pacheco-Peña, M. Beruete, I.V. Minin, O.V. Minin, Multifrequency focusing and wide angular scanning of terajets, Opt. Lett. 40 (2) (Jan. 2015) 245, https://doi.org/10.1364/OL.40.000245.
[23] I.V. Minin, O.V. Minin, Y.E. Geints, Localized EM and photonic jets from non-spherical and non-symmetrical dielectric mesoscale objects: Brief review: Localized EM and photonic jets from non-spherical and non-symmetrical... ANNALEN DER PHYSIK 527 (7-8) (2015) 491–497.
[24] S. Hisatake, E. Miyake, Terahertz scanning microscopy with 2λ depth of field based on photonic nanojet generated by a dielectric cuboid probe, Opt. Express 30 (25) (2022) 45303.
[25] W. R. Folks, S. K. Pandey, and G. Boreman, "Refractive Index at THz Frequencies of Various Plastics," in: Optical Terahertz Science and Technology, Mar. 2007, p. MD10. doi: 10.1364/OTST.2007.MD10.
[26] T. Shimizu, Y. Kawahara, S. Akasaka, Y. Kogami, Complex permittivity measurements of a PTFE substrate in W band by the cut-off circular waveguide method, *2011 China-Japan Joint Microwave Conference*, Apr. (2011) 1–4.

[27] S. Sahin, N.K. Nahar, K. Sertel, Dielectric Properties of Low-Loss Polymers for mmW and THz Applications, J. Infrared, Millimeter, Terahertz Waves 40 (5) (May 2019) 557–573, https://doi.org/10.1007/s10762-019-00584-2.
[28] Z. Chen, A. Taflove, V. Backman, Opt. Express 12 (2004) 1214.
[29] X. Li, Z. Chen, A. Taflove, V. Backman, Opt. Express 13 (2005) 526.
[30] V. Pacheco-Peña, M. Beruete, I.V. Minin, O.V. Minin, Terajets produced by dielectric cuboids, Appl. Phys. Lett. 105 (8) (2014) 1–5, https://doi.org/10.1063/1.4894243.
[31] J. Delgado-Notario, J. Velazquez-Perez, Y. Meziani, K. Fobelets, Sub-THz Imaging Using Non-Resonant HEMT Detectors, Sensors 18 (2) (Feb. 2018) 543.
[32] J. Calvo-Gallego, J.A. Delgado-Notario, J.E. Velázquez-Pérez, M. Ferrando-Bataller, K. Fobelets, A.E. Moussaouy, Y.M. Meziani, Numerical Study of the Coupling of Sub-Terahertz Radiation to n-Channel Strained-Silicon MODFETs, Sensors 21 (3) (Jan. 2021) 688.
[33] J.A. Delgado Notario, E. Javadi, J. Calvo-Gallego, E. Diez, J.E. Velázquez, Y. M. Meziani, K. Fobelets, Sub-Micron Gate Length Field Effect Transistors as Broad Band Detectors of Terahertz Radiation, Int. J. Hi. Spe. Ele. Syst. 25 (03n04) (2016) 1640020.
[34] J. W. Goodman, Introduction to Fourier Optics, 4th ed. Macmillan Learning, 2017. [Online]. Available: https://www.macmillanlearning.com/college/us/product/Introduction-to-Fourier-Optics/p/1319119166.
[35] L. Yue, et al., A Millimetre-Wave Cuboid Solid Immersion Lens with Intensity-Enhanced Amplitude Mask Apodization, J. Infrared, Millimeter, Terahertz Waves 39 (6) (Jun. 2018) 546–552, https://doi.org/10.1007/S10762-018-0479-1/FIGURES/3.
[36] I.V. Minin, O.V. Minin, Terahertz artificial dielectric cuboid lens on substrate for super-resolution images, Opt. Quantum Electron. 49 (10) (Oct. 2017) 1–9, https://doi.org/10.1007/S11082-017-1165-6/FIGURES/4.